Journal of Solid State Chemistry 182 (2009) 1430–1437

Contents lists available at ScienceDirect

Journal of Solid State Chemistry

journal homepage: www.elsevier.com/locate/jssc

Incorporation of Znq_2 complexes into mesoporous silica and their transparent polymer luminescent nanocomposites

Yaying Du [a], Yuqin Fu [b], Yongli Shi [a], Xiaodan Lü [a], Changli Lü [a,*], Zhongmin Su [a]

[a] College of Chemistry, Northeast Normal University, Changchun 130024, PR China
[b] College of Life Sciences, Jilin Agricultural University, Changchun 130118, PR China

ARTICLE INFO

Article history:
Received 25 July 2008
Received in revised form
19 January 2009
Accepted 26 January 2009
Available online 5 February 2009

Keywords:
Znq_2 complex
Mesoporous silica
Fluorescence
Polymer
Transparent nanocomposites

ABSTRACT

Znq_2–functionalized colloidal mesoporous silicas (Znq_2–CMS)/polymer transparent nanocomposites were prepared by in situ bulk polymerization. CMS nanoparticles or nanorods with hydroxyl-, mercapto- and sulfonic-functionalized interiors were obtained by different synthetic routes in the nanosize dimensions between 50 and 500 nm. The luminescent Znq_2 complex was successfully introduced in the pores of different mesoporous silicas by chemical adsorption as the driving force. The different internal circumstances of mesoporous silicas had an obvious effect on the luminescence and lifetime of Znq_2 complex. The transparent fluorescent nanocomposites were fabricated from different Znq_2–CMS and suitable monomers. The Znq_2–CMS were uniformly dispersed in the polymer matrix without evident aggregation. The photoluminescence properties of Znq_2–CMS in the transparent matrix exhibited a dependence on the inner surrounding of CMS due to the interaction between Znq_2–CMS and polymers. The maximum emission peak of the nanocomposites had a red-shift of 28 nm as compared to pure Znq_2–CMS.

© 2009 Elsevier Inc. All rights reserved.

1. Introduction

Mesoporous silica has attracted much research interest in recent years because of the possibility of tailoring the pore structure, framework composition, and morphologies over a wide range [1–3]. Many potential applications arise from the potential properties of these high surface area materials. The wall surface of mesoporous silica can be modified with proper organic functional groups and provide accessibility for anchoring other substances. Accordingly, host–guest complexes have been synthesized from mesoporous silica for such purposes as catalysis [4–7], sensors [8], adsorption [9,10], electronic devices [11–14], optical applications [15], controlled release and drug delivery systems [16–19]. Moreover, the immobilization of luminary on a rigid support is a very important way to prepare new solid luminescent materials which show special photonic behavior. A number of studies have focused on the incorporation of luminary into mesoporous silica. For examples, semiconductor nanocrystals including CdSe [20], ZnS [21,22], CdS [23,24] and so on, confined in mesopore environment show special photonic behavior which is different from that of each pure component. Mesoporous silica-based molecular sieves or zeolites encapsulated with dye molecules and conjugated polymers have been reported [25–28]. The rare-earth complexes such as cerium (III) complex [29], europium (III) chelate with β-diketonate [30] and tris (2,2′-bipyridine) ruthenium (II) [31] have been immobilized in the mesoporous materials. The approaches show that the promising luminescent properties can be obtained by linking the rare-earth complexes to the mesoporous materials. Zhao et al. [32] reported a new method to fabricate the full-color phosphor thin films by incorporating Eu^{3+}, Tb^{3+} complexes into the mesophase silica thin films. Now, extensive research work is going on achieving full color displays based on organic light-emitting diodes (OLEDS). Aluminum tris (8-hydroxyquinoline) as one of the most stable fluorescent solid-state materials has been introduced into the pores of mesoporous silica, and this hybrid luminescent solid material displays greatly promising applications in novel optoelectronic devices [33–35]. Recently, the boron 8-hydroxyquinolinate complexes with the blue emission have been formed by ship-in-a-bottle synthesis inside zeolites via a strategy based on the thermally promoted deboronation of framework boron zeolites [36]. It has been found that the luminescence properties and lifetime of the quinolinate complexes can be strongly modulated by the zeolite host.

As a type of highly luminescent and electroluminescent material, bis(8-hydroxyquinoline) zinc (II) (Znq_2) is becoming the subject of intense interest because of its use in low-voltage organic light-emitting devices (OLEDs) [37,38]. The control of the structural symmetry of the corresponding metal chelates may offer a route to high efficiency and low operating voltage small molecule OLEDs. In this work, the Znq_2 was successfully

* Corresponding author. Fax: +86 43185098768.
E-mail addresses: fuyuqin@yahoo.cn (Y. Fu), lucl055@nenu.edu.cn (C. Lü).

0022-4596/$ - see front matter © 2009 Elsevier Inc. All rights reserved.
doi:10.1016/j.jssc.2009.01.029

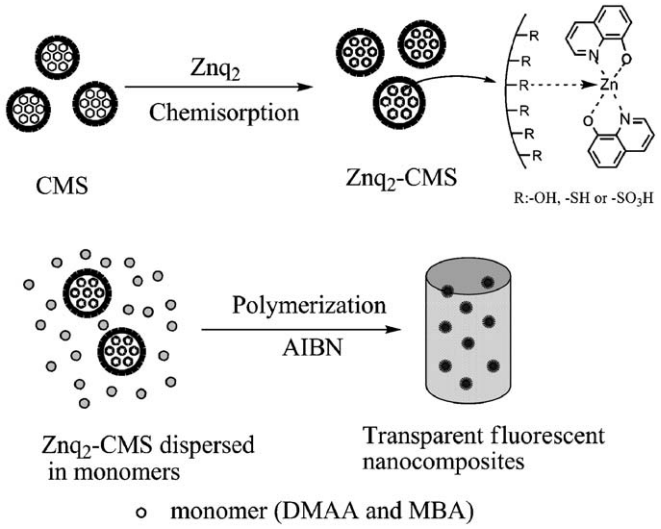

Scheme 1. Synthetic scheme for the preparation of Znq_2–CMS and their transparent polymer nanocomposites.

incorporated into the mesoporous silica with different nanosize dimensions and the effect of the interior circumstances of mesoporous silica on the optical properties of Znq_2 was studied. It is also the first report to effectively tailor the luminescence properties of Znq_2 by the host–guest interactions in the mesoporous silica. In addition, to realize the processability of these fluorescent mesoporous silica used as materials, it is necessary and alternative to construct nanocomposites by the composite and assembly of these functional mesoporous silica in polymer matrix. So the resultant Znq_2–functionalized colloidal mesoporous silicas (Znq_2–CMS) with good luminescence were also incorporated into polymer matrix to fabricate a series of transparent fluorescent nanocomposites by in situ bulk polymerization. These polymer luminescent nanocomposites have greatly promising applications in novel optoelectronic devices. Scheme 1 shows the schematic diagram for the synthesis of Znq_2–CMS and their transparent polymer nanocomposites by in situ free radical bulk polymerization.

2. Experimental

2.1. Materials

8-Hydroxyquinoline, zinc acetate dihydrate, hexadecyltrimethylammonium bromide (CTAB), tetraethyl orthosilicate (TEOS, 98%), N, N′-methylenebisacrylamide (MBA) and triethylamine were all of analytical grade reagents and were used without further purification. 3-Mercaptopropyltrimethoxy-silane (MPTS, 95%) was obtained from Aldrich. Azodisisobutyronitrile (AIBN) was recrystallized in ethanol. N, N-dimethylacrylamide (DMAA) was purchased from TCI and was distilled under reduced pressure before use.

2.2. Synthesis of different mesoporous silicas

Three kinds of CMS with different morphologies and interior circumstances were prepared according to the procedure described in the literature [39]. CMS with hydroxyl groups (CMS–OH, spherical) were synthesized by the following reaction: 2.625 mL 2 M NaOH (5.25×10^{-3} mol) and 0.765 g CTAB (2.1×10^{-3} mol) were dissolved in 360 mL water (19.98 mol), the resulting solution was heated to 80 °C, then 3.75 mL TEOS (1.68×10^{-2} mol) was added under stirring and the reaction was kept at this temperature for two hours. CMS with mercapto groups (CMS–SH, rod-like) were synthesized as above procedure, just 0.318 mL MPTS (1.68×10^{-3} mol) was added in company with TEOS. CMS with sulfonic acid groups (CMS–SO_3H, rod-like) were obtained by the oxidation of CMS–SH with concentrated hydrogen peroxide (33%) after template extraction. The obtained samples were separated by centrifugation at 9000 rpm for 20 min. The solids were immediately taken up in distilled water, sonicated, and washed for several times. Template extraction was performed with 15 mL conc. HCl in 120 mL ethanol. Usually, one gram of sample was treated two to three times with 100 mL of the extraction solution by sonication for 30 min. Subsequent washing was performed as described above.

2.3. Preparation of bis(8-hydroxyquinoline) zinc(II) complex (Znq_2)

The typical synthetic process is as follow [40]: an aqueous solution (40 mL) of zinc acetate dihydrate (0.01 mol) was added dropwise to the acetone solution (80 mL) of 8-hydroxyquinoline (0.02 mol) and triethylamine (0.02 mol) under stirring. After refluxing the mixture at 50–60 °C for 2 h, a crude product would precipitate from the solution. The precipitates were collected by centrifugation (6000 rpm, 10 min) and washed with acetone and deionized water for several times, respectively. The composition of the product was confirmed to be Zn $(C_9H_6ON)_2 \cdot 2H_2O$ (Znq_2) by elemental analysis.

2.4. Adsorption of Znq_2 complex onto mesoporous silica

The adsorption of Znq_2 complex onto mesoporous silica was conducted by soaking the dried mesoporous silicas in absolute ethanol solution of Znq_2 complex at room temperature for 12 h. In a typical synthesis, 0.25 g of CMS was suspended in 50 mL ethanol solution of Znq_2 (5×10^{-3} mol L^{-1}). The resulting Znq_2–CMS solids (Znq_2–CMS–OH, Znq_2–CMS–SH and Znq_2–CMS–SO_3H) were collected by centrifugation and washed several times with deionized water until the eluent turned colorless. The products were then dried under reduced pressure for 12 h.

2.5. Preparation of transparent Znq_2–CMS /polymer bulk nanocomposites

The mesoporous silicas with different morphologies were introduced into polymer matrix by in situ bulk polymerization. 1 wt% of Znq_2–CMS was dispersed in monomer mixtures of DMAA and MBA (crosslinking agent) under ultrasonic vibration. The weight ratio of DMAA:MBA was fixed at 100:5. Subsequently, 0.4% w/w of 2, 2′-azobisisobutyronitrile (AIBN) was added to the above suspension and prepolymerization was carried out at 75 °C for 10 min after degassing. Finally, the polymerization were carried out at 50 °C for 12 h, 70 °C for 2 h, 80 °C for 2 h, 90 °C for 1 h, 100 °C for 1 h and 110 °C for 1 h, and then a series of transparent nanocomposite rods were obtained.

2.6. Characterization

Transmission electron microscopy (TEM) was carried out using a JEOL-2021 microscope that was operated at 200 kV with the sample deposited on a holey carbon copper grid. Scanning electron microscopy (SEM) was carried out with an XL-30 ESEM FEG SEM (FEI COMPANY). Nitrogen (N_2) adsorption/desorption isotherms were measured by using a Nova l000 analyzer with

nitrogen. The samples were outgassed for 6 h at 100 °C before the measurements. Surface areas were calculated by the Brunauer–Emmett–Teller (BET) method and pore sizes by the Barrett–Joyner–Halenda (BJH) methods. The content of zinc ions in Znq_2–CMS was detected by inductively coupled plasma–atomic emission spectrometry (ICPAES) method on a LEEMAN Prodigy High Dispersion ICP. Raman spectrum was taken with inVia Raman microscope (633 nm). Photoluminescence spectra were recorded on a Cary Eclipse fluorescence spectrometer equipped. Luminescence lifetime were measured with a Lecroy Wave Runner 6100 digital oscilloscope (1 GHz) using a 355 nm laser radiation (pulse width = 4 ns) as the excitation source (ContinuumSunlite OPO). Mean (average) fluorescence lifetime $\langle\tau\rangle$ for biexponential iterative fitting were calculated from the decay times and the pre-exponential factors using the relation $\langle\tau\rangle = (b_1\tau_1+b_2\tau_2)$.

3. Results and discussion

Fig. 1 shows the TEM micrographs of CMS samples. The inset in the micrograph is an amplification image of a single CMS in which a hexagonal array of ordered mesopores is clearly visible. The diameter is 100–200 nm for the mesoporous sphere (CMS–OH) (Fig. 1a), while the diameter of mesoporous rods (CMS–SO_3H) is highly uniform with a size between 60 and 70 nm while the length varies between 300 and 500 nm (Fig. 1b), and this result is identical with previous report [39]. TEM morphology of CMS–SH is similar to that of CMS–SO_3H (not shown). Znq_2–CMS were prepared by soaking the dried mesoporous silicas in absolute ethanol solution of Znq_2 complex. The mesoporous structure and morphology of CMS can be substantially maintained after the deposition of the Znq_2. However, the Znq_2 complex within the host channel cannot be well resolved from the TEM image (not shown) contrast of the channel and the wall structure of the host. Existence of the Znq_2 complex within the nanochannels of the host, however, can be confirmed by the following nitrogen sorption experiments and ICPAES analysis.

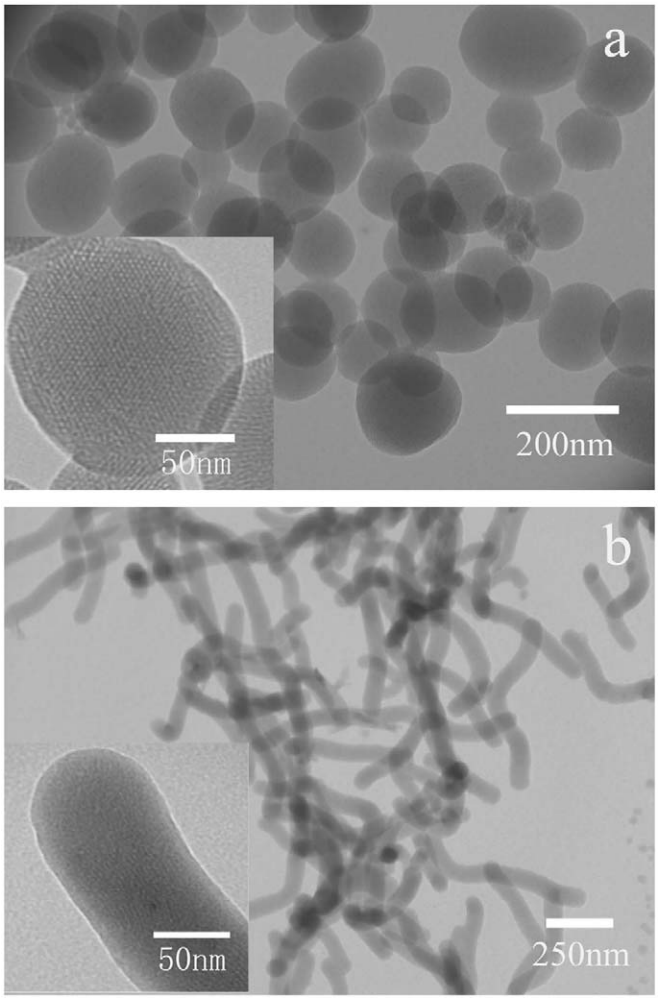

Fig. 1. TEM images of (a) CMS–OH and (b) CMS–SO_3H. The inset is the expanded image of a single nanoparticle.

Fig. 2 displays the nitrogen adsorption/desorption isotherms and pore size distribution for CMS and Znq_2–CMS. All samples show the type-IV isotherms according to the IUPAC classification [41]. A well-defined step at intermediate relative pressure ($0.2 < P/P_0 < 0.4$ in Fig. 2a, $0.1 < P/P_0 < 0.3$ in Fig. 2b and Fig. 2c) is related with the filling of the mesopores due to capillary condensation of N_2 inside the mesopores. The nitrogen adsorption isotherms of CMS–OH and Znq_2–CMS–OH (Fig. 2a) feature a pronounced hysteresis loop at a relative pressure of about 0.3, which is characteristic of a highly ordered mesoporous structure. By using BET and BJH methods, the calculated specific area and pore size as well as the pore volume are given in Table 1. BET surface area and total pore volume of Znq_2–CMS obviously decreased as compared to bare CMS. This phenomenon originates from the dispersion of the Znq_2 complexes on the surface of the parent CMS material since these complexes dispersed inside the channel would enhance the roughness of the pore surfaces and then make the surface area and pore volume of these materials much smaller than those of the parent CMS materials. ICPAES analyses exhibit that the contents of Znq_2 complexes are 2.27, 5.81 and 6.62 wt% for Znq_2–CMS–OH, Znq_2–CMS–SH and Znq_2–CMS–SO_3H, respectively (see Table 1). These results indicate that the Znq_2 complex has been successfully introduced into the CMS and the different interior circumstances could influence the adsorption amount of the Znq_2 due to the host–guest interaction.

Raman spectroscopy is an excellent tool to detect thiol and sulfonic acid groups due to their relatively intensive Raman scattering. We compared the Raman signatures of the CMS samples before and after functionalization with Znq_2 (Fig. 3). The band at 2583 cm^{-1} in the CMS–SH sample (Fig. 3a) is assigned to the ν_{SH} stretching mode of the mercaptopropyl segment [42]. However, as the Znq_2 was introduced into CMS–SH, the signature obviously decreases, at the same time, we can also see the appearance of the new bands at 1584 and 1376 cm^{-1} in comparison to the unfunctionalized sample. These vibrations are assigned to the characteristic absorptions of quinoline group in Znq_2 [43]. The Raman spectrum in Fig. 3b shows an intensive band at 1049 cm^{-1} for the symmetric vibration mode of the –SO_3H group in the CMS–SO_3H sample [44]. The signature obviously weakens in the Znq_2-containing samples (Znq_2–CMS–SO_3H). The bands at 1328 and 1460 cm^{-1} in Znq_2–CMS–SO_3H should correspond to the characteristic absorptions of quinoline and phenyl groups in Znq_2 [43]. The obvious decrease in the signature for both the –SH and –SO_3H groups shows that there is a strong interaction between the Znq_2 and the –SH or –SO_3H groups in the mesoporous surface. The above ICPAES results also show that the zinc ion contents in Znq_2–CMS–SH and Znq_2–CMS–SO_3H is higher than that of Znq_2–CMS–OH.

Fig. 4 shows the solid state PL spectra of Znq_2–CMS–OH (a), Znq_2–CMS–SH (b) and Znq_2–CMS–SO_3H (c) at the excitation wavelength of 350 nm. The normalized PL spectra of Znq_2–CMS and Znq_2 are also shown in inset of Fig. 4. It can be seen that Znq_2 exhibits a maximum PL emission at 491 nm. After Znq_2 was introduced into CMS–SH and CMS–SO_3H, the fluorescent emission peaks of Znq_2–CMS–SH and Znq_2–CMS–SO_3H samples have a

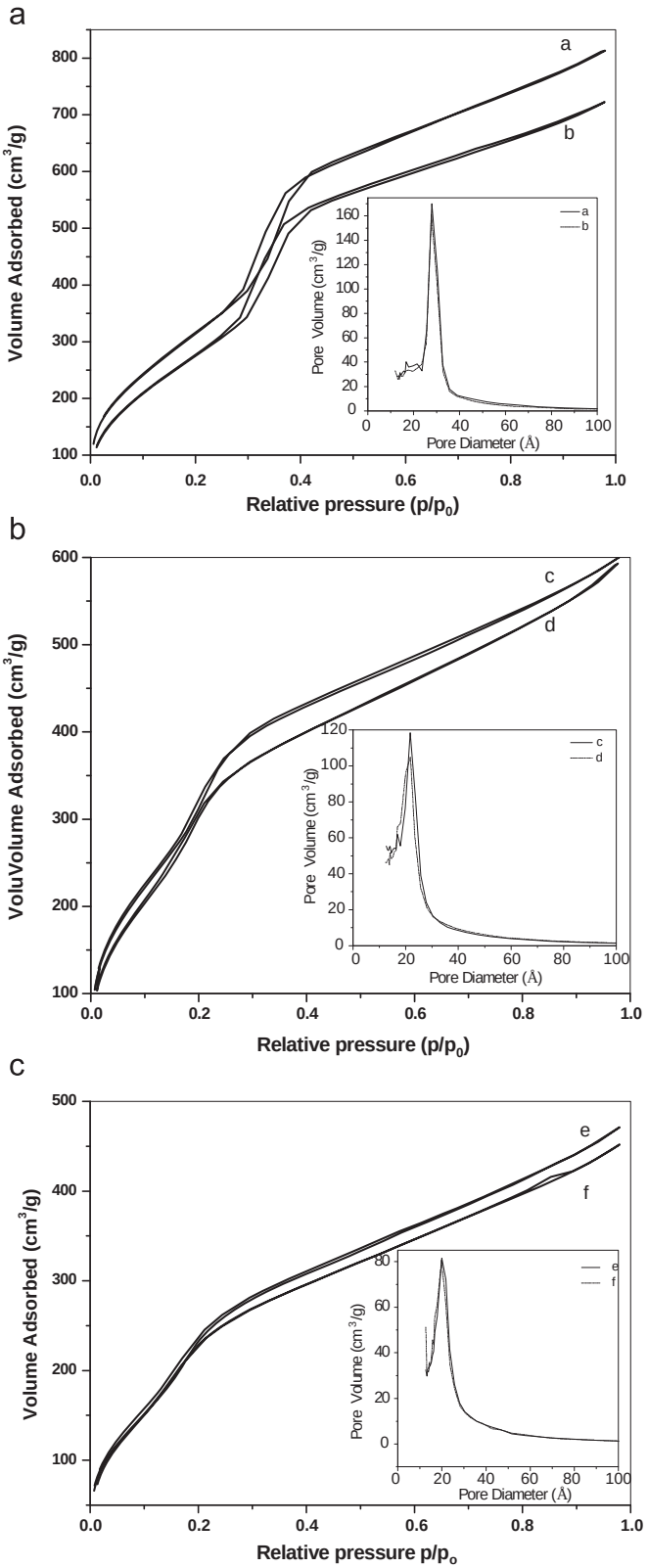

Fig. 2. Nitrogen adsorption–desorption isotherms of CMS–OH (a), Znq_2–CMS–OH (b), CMS–SH(c), Znq_2–CMS–SH (d), CMS–SO_3H (e) and Znq_2–CMS–SO_3H (f). The insets are the corresponding BJH pore distributions.

slight red-shift of about 2 and 3 nm, respectively, while for Znq_2–CMS–OH samples, there is no obvious change for the maximum PL emission. It can be also observed that all the PL spectra of the Znq_2-containing CMS samples become broader than that of pure Znq_2, in particular, this variation trend becomes more obvious for the Znq_2–CMS–SH and Znq_2–CMS–SO_3H samples. This result indicates that the interior circumstances of CMS have an effect on the luminescent properties of Znq_2 due to the host–guest interaction. In addition, the photoluminescence intensity of the Znq_2–CMS obviously decreases with the change of the interior functionalized organic groups in CMS, which is well in accordance with the results of the lifetime decay dynamics for different Znq_2–CMS and pure Znq_2 complex solids. Fig. 5 presents the luminescence decay curves for the pure Znq_2 and Znq_2–CMS solid samples. The pure Znq_2 exhibits a single exponential PL decay with a lifetime of 25 ns. However, the decay times of Znq_2 loaded in CMS are fitted by biexponential decay. The fast and slow components are 11 (96%) and 26 ns (4%) for the Znq_2–CMS–SH, 6 (97%) and 15 ns (3%) for the Znq_2–CMS–SO_3H, and 23 (94%) and 11 ns (6%) for the Znq_2–CMS–OH, respectively. The average decay times of the three samples are 11.6, 6.3 and 22.3 ns, respectively (see Table 2). It clearly reveals that the decay times for the Znq_2 loaded in CMS become shorter with the increasing interaction between the Znq_2 and mesopore surface. The above results show that the Znq_2 molecules are difficult to aggregate in the mesoporous channels of CMS due to the strong steric confinement effect of the local environment, and thus the Znq_2 molecules should be highly dispersed and be presented as similar as monomers. The interactions between the Znq_2 molecules and the organic groups in CMS occupy dominant station compared with the interactions between Znq_2 molecules. The fluorescent characters are mostly affected by the former. The stronger the interaction, the lower is the intensity of the fluorescent emission of Znq_2. It should be noted that this interaction is from the attack of the functional groups (*R*) to the Zn atom of Znq_2, which results in the formation of the weak Zn–*R* coordination bond (as shown in Scheme 1). It is known that the cation exchange capacity of pure silica originating from the weakly acid silanol groups [45] is rather low, resulting in poor binding efficiency of heavy metal ions. Because the binding ability of –SH and –SO_3H with zinc atom is stronger than –OH, the interaction between the Znq_2 complex and the –SH or –SO_3H is stronger than –OH in CMS, the decrease in the PL intensity is more obvious for the Znq_2–CMS–SH and Znq_2–CMS–SO_3H samples. The Znq_2–CMS–SO_3H exhibits the lowest fluorescent emission intensity in the three samples possibly because of the relative strong pH value of –SO_3H groups.

The different fluorescent Znq_2–CMS were incorporated into the polymer matrix to prepare a series of transparent nanocomposites by in situ bulk polymerization. The DMAA and MBA (crosslinking agent) were selected as the comonomers to prepare the polymer matrix because these monomers and their corresponding polymers have good compatibility with the CMS. It is more important that the polymer matrix obtained from DMAA and MBA has the close refractive index (1.49) to that (~1.49) of CMS. The refractive index matching between the polymer matrix and fillers could suppress the light scattering and ensure that the resulting nanocomposites have good transparency in the visible region regardless of the size and shape of the fillers.

Fig. 6a illustrates the optical photographs of the pristine polymer rod and the fluorescent nanocomposite rods containing 1 wt% Znq_2–CMS. It can be seen that the bulk nanocomposites possess good transparency owing to the good dispersibility of Znq_2–CMS and the matching of refractive index between the polymer matrix and Znq_2–CMS. The SEM images (Fig. 7) of the fracture surface of the nanocomposites show that all the Znq_2–CMS with round or rod shapes are uniformly dispersed in the polymer matrix without obvious aggregation. In addition, we can also observe that the CMS are well embedded in the polymer matrix, indicating that there is a strong interaction between the

Table 1
Some properties and morphologies of different CMS and Znq_2-CMS.

Sample	S_{BET}[a] ($m^2 g^{-1}$)	V_t[b] ($cm^3 g^{-1}$)	D_{BJH}[c] (nm)	Morphology	Zn content (wt%)	$Znq_2 \cdot 2H_2O$ content (wt%)
CMS–OH	1207	1.256	4.1625	Round particles	–	–
Znq_2–CMS–OH	1072	1.116	4.1643	Round particles	0.38	2.27
CMS–SH	1270	0.9278	3.0467	Fibers	–	–
Znq_2–CMS–SH	1203	0.9162	2.9221	Fibers	0.97	5.81
CMS–SO_3H	922	0.7280	3.1588	Fibers	–	–
Znq_2–CMS–SO_3H	886	0.6982	3.1521	Fibers	1.11	6.62

[a] BET surface area.
[b] Total pore volume.
[c] Average pore diameter calculated using BJH method.

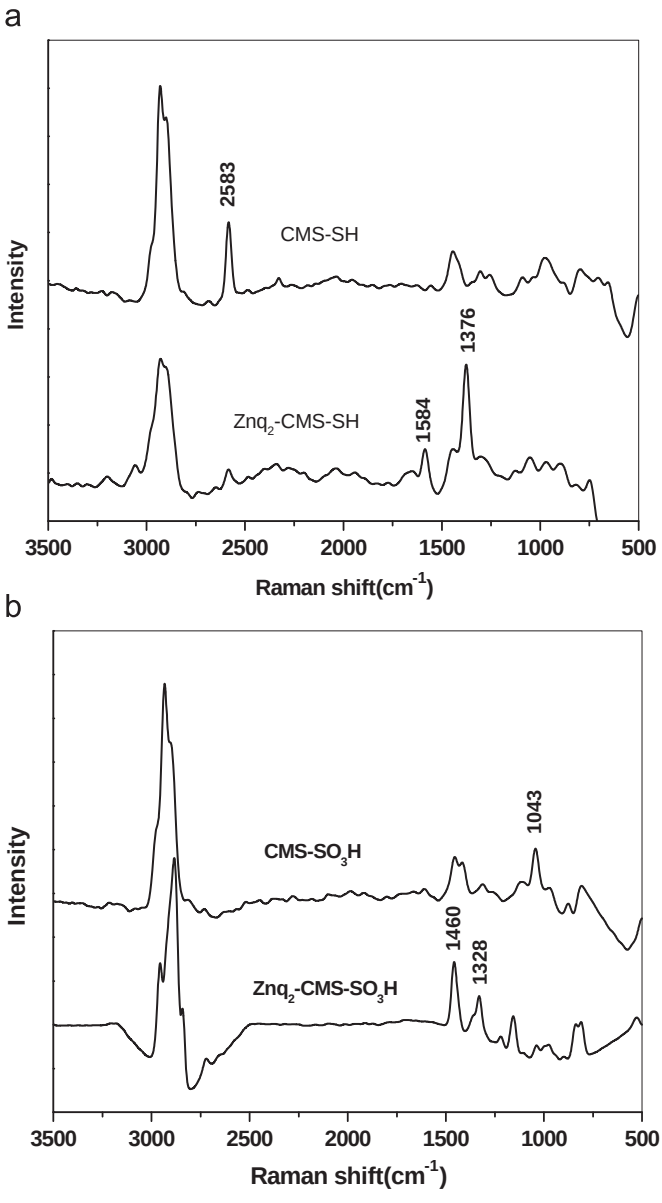

Fig. 3. Raman spectra of (a) CMS–SH and Znq_2–CMS–SH and (b) CMS–SO_3H and Znq_2–CMS–SO_3H.

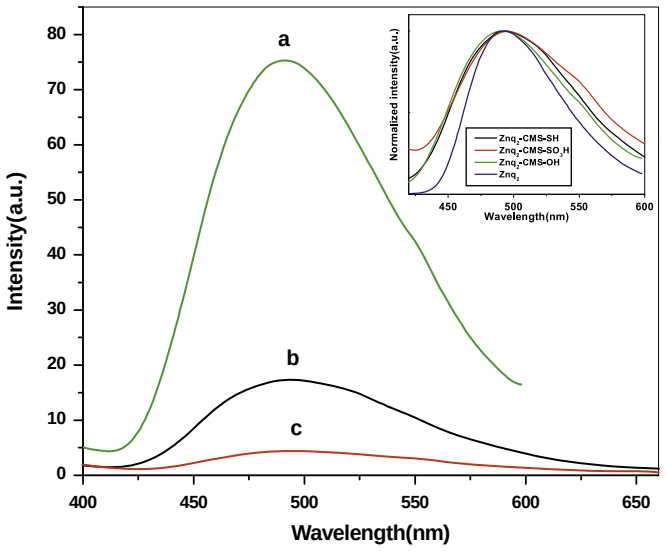

Fig. 4. PL spectra of (a) Znq_2–CMS–OH, (b) Znq_2–CMS–SH and (c) Znq_2–CMS–SO_3H. The inset is the normalized PL spectra of Znq_2 and different Znq_2–CMS.

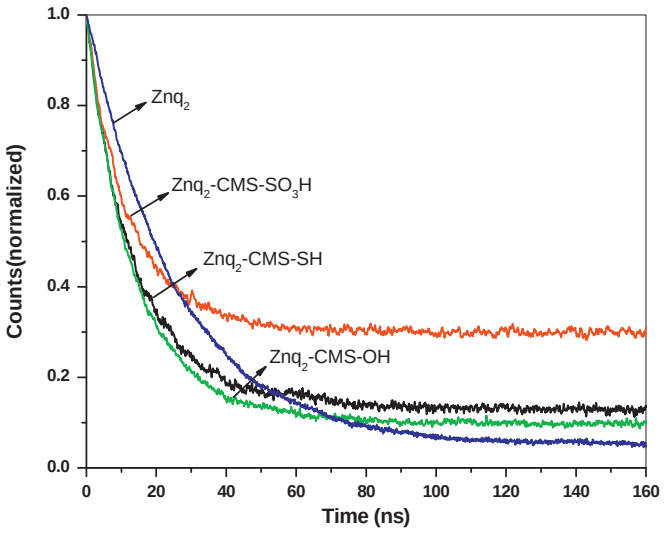

Fig. 5. PL decay curves of Znq_2 and different Znq_2–CMS.

polymer matrix and CMS, and it may play an effect on the fluorescent properties of the resulting nanocomposites.

The PL spectra of the polymer matrix and different Znq_2–CMS (1 wt%)/polymer nanocomposites are shown in Fig. 8. The positions of maximum excitation peak (λ_{ex}) and maximum emission peak (λ_{em}) for different nanocomposites are listed in Table 3. It should be noted that the pure polymer matrix obtained from DMAA/MBA presents a blue emission at 400 nm as excited

Table 2
Excitation (λ_{ex}) and emission (λ_{em}) peak positions, and fluorescence decay data for Znq_2 and Znq_2–CMS.

Samples	λ_{ex} (nm)	λ_{em} (nm)	b_1	τ_1 (ns)[a]	B_2	τ_2 (ns)	$\langle\tau\rangle = (b_1\tau_1+b_2\tau_2)$ (ns)[b]
Znq_2	350	491	1	25	–	–	25
Znq_2–CMS–SH	350	493	0.96	11	0.04	26	11.6
Znq_2–CMS–SO_3H	350	494	0.97	6	0.03	15	6.3
Znq_2–CMS–OH	350	491	0.94	23	0.06	11	22.3

[a] The decay time of the solid-state samples was obtained from the decay curves, which simulated by using the multiexponetial model $I(t) = \sum_{i=1}^{n} \alpha_i \exp(-t/\tau_i)$ The excitation wavelength is 355 nm. The Znq_2 exhibits a single exponential decay and Znq_2–CMS samples present the biexponential fluorescence decay.
[b] Average fluorescence lifetime.

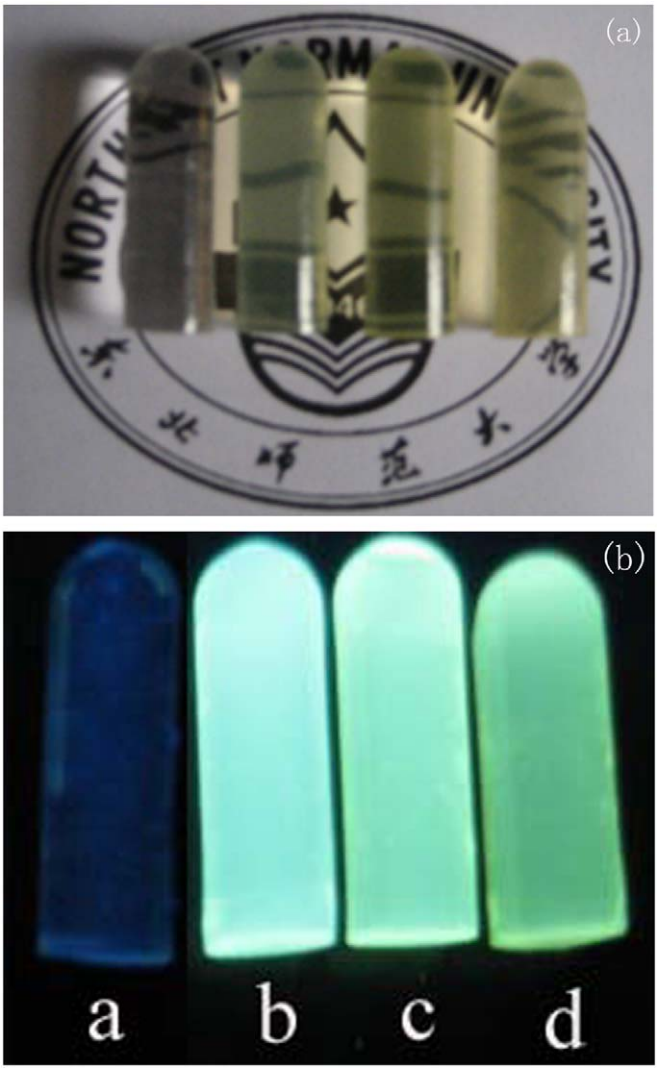

Fig. 6. Photographic images of Znq_2–CMS/polymer transparent nanocomposites (a) under daylight and (b) under a UV lamp with samples from left to right: polymer, Znq_2–CMS–OH/polymer, Znq_2–CMS–SH/polymer and Znq_2–CMS–SO_3H/polymer.

by 350 nm. This emission band may be attributed to the PDMAA segments in the polymer [46]. When Znq_2–CMS were embedded in the polymer matrix, the nanocomposites exhibit a complicated fluorescent emission property which depends on the inner surrounding of CMS. The emission and excitation peaks of the nanocomposites have an obvious red-shift when compared with

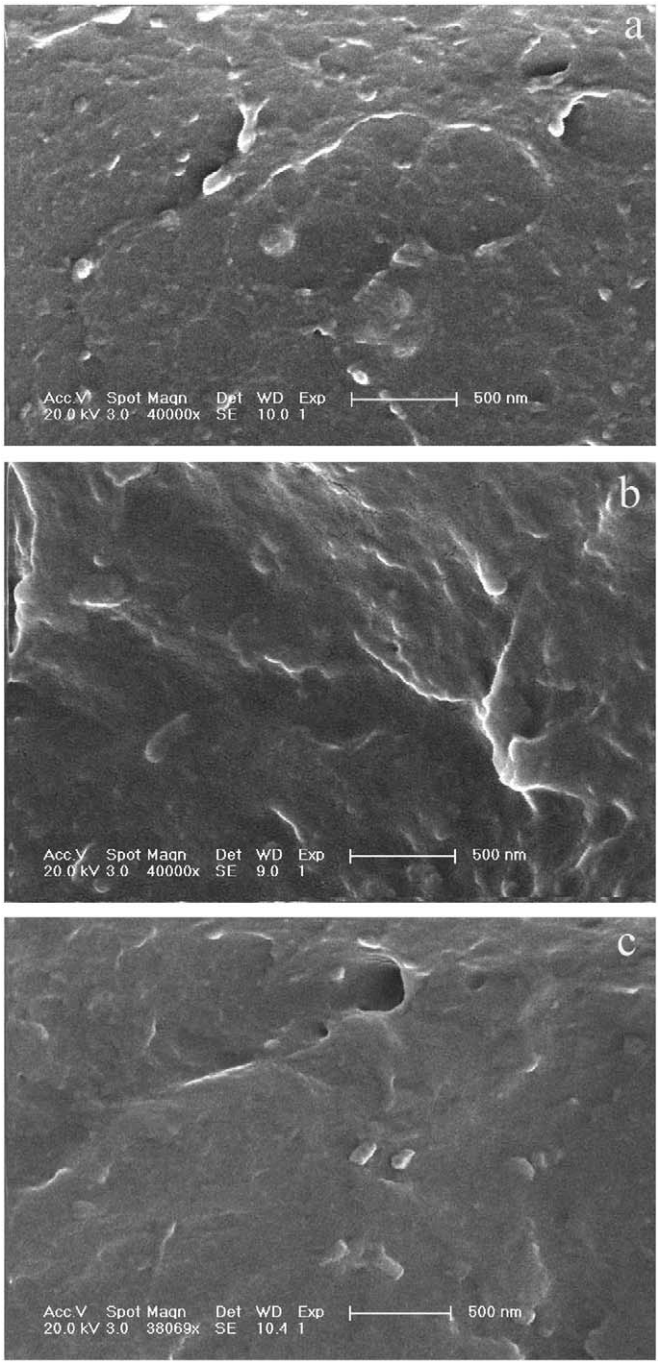

Fig. 7. SEM images of different nanocomposites with (a) Znq_2–CMS–OH, (b) Znq_2–CMS–SH and (c) Znq_2–CMS–SO_3H.

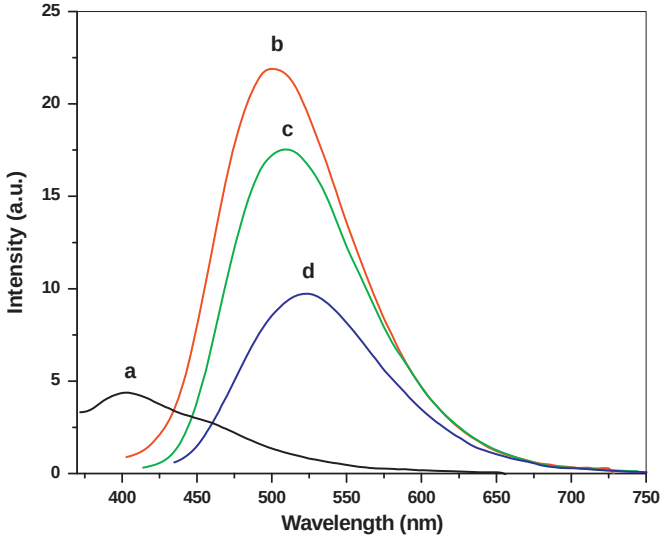

Fig. 8. PL spectra of polymer matrix (a) and different nanocomposites with Znq_2–CMS–OH (b), Znq_2–CMS–SH (c) and Znq_2–CMS–SO_3H (d).

Table 3
Photoluminescence properties of different Znq_2–CMS/polymers nanocomposites.

Samples	Composition of nanocomposites	λ_{ex} (nm)[b]	λ_{em} (nm)[c]	τ (ns)
a	Polymer[a]	350	400	–
b	Znq_2–CMS–OH (1 wt%)/polymer	379	501	28
c	Znq_2–CMS–SH (1 wt%)/polymer	390	509	25
d	Znq_2–CMS–SO_3H (1 wt%)/polymer	411	522	18

[a] The polymer is assigned to polymer matrix obtained from copolymerization of monomers DMAA/MBA.
[b] λ_{ex} is the position of maximum excitation peak.
[c] λ_{em} is the position of maximum emission peak.

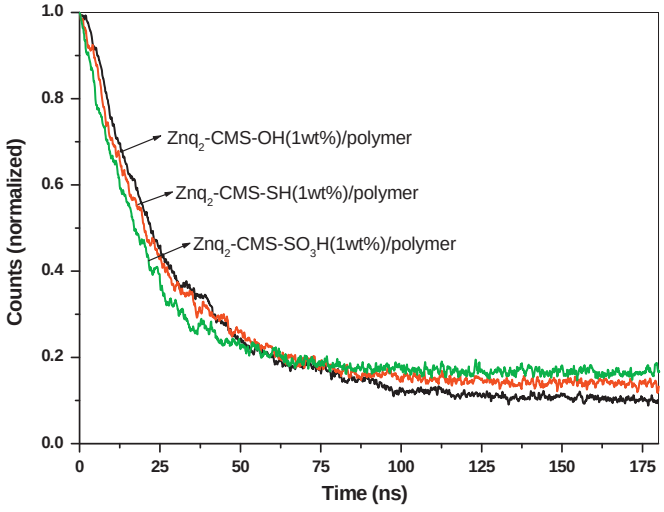

Fig. 9. PL decay curves of different Znq_2–CMS (1 wt%)/polymer nanocomposites.

both of the polymer matrix and the corresponding Znq_2–CMS. The fluorescence intensities of the samples also decrease with the increasing interaction between Znq_2 and CMS and have the same variation trend as the pure Znq_2–CMS (see Fig. 4). The PL decay curves (Fig. 9) show that all the nanocomposites exhibit a single exponential PL decay with the lifetimes of 28, 25 and 18 ns for Znq_2–CMS–OH(1 wt%)/polymer, Znq_2–CMS–SH (1 wt%)/ polymer and Znq_2–CMS–SO_3H(1 wt%)/polymer samples, respectively (see Table 3). This result is obvious different from the biexponential decay character of Znq_2–CMS, and moreover, it should be noted that the lifetime of the nanocomposites increases compared with the corresponding Znq_2–CMS sample (see Table 2). Some monomers penetrated into the mesoporous channel of CMS before polymerization and partially weakened the interaction of Znq_2 complex with the –SH or –SO_3H functional groups in CMS. Thus, it is possible that the interaction between Znq_2–CMS and PDMAA segments in polymer matrix with a blue emission results in the local environment change of Znq_2 complex in CMS channel, which can affect the PL spectra and decay behavior of different nanocomposites. It can be seen that the maximum emission peak (522 nm) of the nanocomposite with Znq_2–CMS–SO_3H has a red-shift of 28 nm as compared to pure Znq_2–CMS–SO_3H (494 nm), indicating that the Znq_2 complex in Znq_2–CMS–SO_3H has stronger interaction with polymer matrix than the others, which may affect the fluorescent properties of Znq_2 in CMS. The above SEM images also indirectly show this strong interaction because CMS are embedded in polymer matrix (the polymer may fill into the mesopores of CMS). In addition, the difference of Znq_2 content of CMS in the nanocomposites may be another reason which results in the change of the fluorescent properties of composites because the Znq_2 content in Znq_2–CMS–SO_3H is the highest. In the previous report, we also found the dependence of the content of luminary in similar polymer matrix on the fluorescent properties of composites [44]. Further study will be required to well understand the mechanism affecting the photoluminescence properties of the nanocomposites. Fig. 6b presents the PL images of the different nanocomposites rods excited by an ultraviolet lamp at 360 nm. The strong PL emission can be observed and their fluorescent emission colors are in accordance with the PL spectra (Fig. 8).

The thermal stability of the nanocomposites was characterized by thermogravimetric analysis (TGA). Fig. 10 presents the TGA curves for the polymer matrix and bulk nanocomposites at a heating rate of 20 °C min^{-1} under N_2 flow from 50 to 850 °C. As the Znq_2–CMS were incorporated into the polymer matrix to form bulk nanocomposites, the resulting nanocomposites have a similar thermal stability as the polymer matrix except the sample with Znq_2–CMS–SH. The reason may be that the partially mercapto groups in CMS result in the chain transfer termination

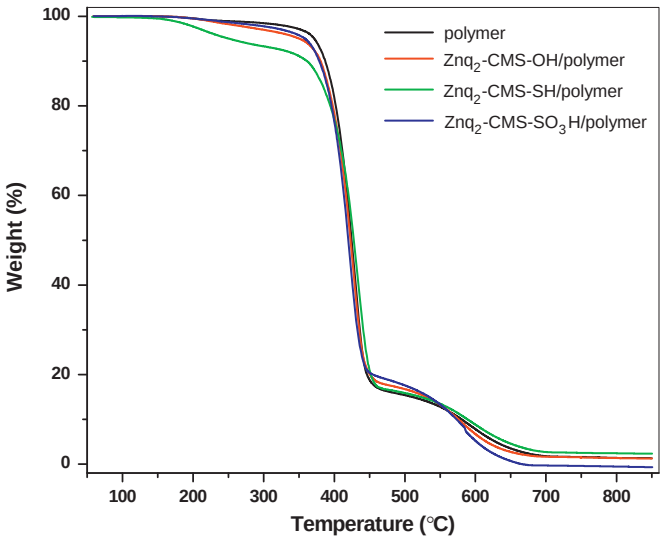

Fig. 10. TGA curves of polymer matrix and different nanocomposites.

in the process of free radical polymerization of monomers filled into the channel of Znq_2–CMS–SH, as a result, a small quantity of polymers with low thermal stability structures was formed nearby/in CMS. Both the pure polymer matrix and different polymer nanocomposites exhibit an initial decomposition temperature of about 200 °C and an obvious weight loss process at about 400 °C. The bulk nanocomposite residues seen in the TGA curves have no obvious change compared with the polymer matrix due to the low content of Znq_2–CMS (1 wt%).

4. Conclusions

In summary, Znq_2 complex was successfully occluded into the mesoporous silica with different inner surroundings by a simple post-chemisorption process. This method can modulate the photophysical properties of Znq_2 by controlling the host–guest interactions between Znq_2 and mesoporous silica. A series of Znq_2–functionalized mesoporous silica (Znq_2–CMS)/polymer fluorescent nanocomposites were prepared by in situ bulk polymerization. These transparent nanocomposites displayed good photoluminescence, and the interaction between the polymer and Znq_2–CMS can also influence the emission spectra of the resulting nanocomposites. These Znq_2–functionalized fluorescent mesoporous silica and their transparent polymer nanocomposites can be potentially used to fabricate multifunctional delivery system and photoelectric devices, respectively.

Acknowledgments

This work was supported by the National Natural Science Foundation of China (no.20704004) and the Training Fund of NENU'S Scientific Innovation Project (NENU-STC07003), NENU-STB-07007, and the Analysis and Testing Foundation of Northeast Normal University.

References

[1] K. Möller, J. Kobler, T. Bein, Adv. Funct. Mater. 17 (2007) 605.
[2] J. Kobler, K. Möller, T. Bein, ACS Nano. 2 (2008) 791.
[3] Y. Wan, D.Y. Zhao, Chem. Rev. 107 (2007) 2821.
[4] A. Stein, B.J. Melde, R.C. Schroden, Adv. Mater. 12 (2000) 1403.
[5] J.Y. Ying, C.P. Mehnert, M.S. Wong, Angew. Chem. Int. Ed. 38 (1999) 56.
[6] I.K. Mbaraka, K.J. McGuire, B.H. Shanks, Ind. Eng. Chem. Res. 45 (2006) 3022.
[7] D.S. Shephard, T. Mashmeyer, B.F.G. Johnson, Angew. Chem. Int. Ed. 36 (1997) 2242.
[8] A.B. Descalzo, R. Martínez-Máôez, F. Sancenón, K. Hoffmann, K. Rurack, Angew. Chem. Int. Ed. 45 (2006) 5924.
[9] X. Feng, G.E. Fryxell, L.Q. Wang, A.Y. Kim, J. Liu, K.M. Kemner, Science 276 (1997) 923.
[10] L. Liu, X. Feng, G.E. Fryxell, L.Q. Wang, A.Y. Kim, M. Gong, Adv. Mater. 10 (1998) 161.
[11] N.R.B. Coleman, M.A. Morris, T.R. Spalding, J.D. Holmes, J. Am. Chem. Soc. 123 (2001) 187.
[12] H. Yang, Q. Shi, B. Tian, Q. Lu, F. Gao, S. Xie, J. Fan, C. Yu, B. Tu, D. Zhao, J. Am. Chem. Soc. 125 (2003) 4724.
[13] T. Abe, Y. Tachibana, T. Uematsu, M. Lwamoto, J. Chem. Soc. Chem. Commun. 16 (1995) 1617.
[14] Y. Han, J.M. Kim, G.D. Stucky, Chem. Mater. 12 (2000) 2068.
[15] B.J. Scott, G. Wirnsberger, G.D. Stucky, Chem. Mater. 13 (2001) 3140.
[16] N.W. Clifford, K.S. Iyer, C.L. Raston, J. Mater. Chem. 18 (2008) 162.
[17] B.G. Trewyn, I.I. Slowing, S. Giri, H.T. Chen, V.S.Y. Lin, Acc. Chem. Res. 40 (2007) 846.
[18] B.G. Trewyn, S. Giri, I.I. Slowing, V.S.Y. Lin, Chem. Commun. (2007) 3236.
[19] M. Vallet-Regí, F. Balas, D. Arcos, Angew. Chem. Int. Ed. 46 (2007) 7548.
[20] H. Parala, H. Winkler, M. Kolbe, A. Wohlfart, R.A. Fischer, R. Schmechel, H. Seggern, Adv. Mater. 12 (2000) 1050.
[21] W.H. Zhang, J.L. Shi, H.R. Chen, Z.L. Hua, D.S. Yan, Chem. Mater. 13 (2001) 648.
[22] W.S. Chae, J.H. Yoon, H. Yu, D.J. Jang, Y.R. Kim, J. Phys. Chem. B 108 (2004) 11509.
[23] S.Z. Wang, D. Choi, S.M. Yang, Adv. Mater. 14 (2002) 1311.
[24] W. Xu, Y. Liao, D.L. Akins, J. Phys. Chem. B 106 (2002) 11127.
[25] G. Schulz-Ekloff, D. Wöhrle, B. van Duffel, R.A. Schoonheydt, Micropor. Mesopor. Mater. 51 (2002) 91.
[26] L. Wang, Y. Liu, F. Chen, J. Zhang, M. Anpo, J. Phys. Chem. C 111 (2007) 5541.
[27] A.Z. Ruiz, H. Li, G. Calzaferri, Angew. Chem. Int. Ed. 45 (2006) 5282.
[28] A.G. Pattantyus-Abraham, M.O. Wolf, Chem. Mater. 16 (2004) 2180.
[29] K. Klier, A.C. Miller, L.L. Zhang, M.K. Hatalis, Chem. Mater. 20 (2008) 1359.
[30] E. DeOliveira, C.R. Neri, O.A. Serra, A.G.S. Prado, Chem. Mater. 19 (2007) 5437.
[31] M. Sohmiya, Y. Sugahara, M. Ogawa, J. Phys. Chem. B 111 (2007) 8836.
[32] D. Zhao, S.J. Seo, B.S. Bae, Adv. Mater. 19 (2007) 3473.
[33] H. Wang, J. Huang, S. Wu, C. Xu, L. Xing, L. Xu, Q. Kan, Mater. Lett. 60 (2006) 2662.
[34] N. Li, X. Li, W. Wang, W. Geng, S. Qiu, Mater. Chem. Phys. 100 (2006) 128.
[35] M. Tagaya, M. Ogawa, Chem. Lett. 35 (2006) 108.
[36] A. Corma, U. Díaz, B. Ferrer, V. Fornés, M.S. Galletero, H. García, Chem. Mater. 16 (2004) 1170.
[37] Y. Hamada, T. Sano, N. Fujita, T. Fujii, Y. Nishio, K. Shibata, Jpn. J. Appl. Phys. 32 (1993) L514.
[38] L.S. Sapochak, F.E. Benincasa, R.S. Schofield, J. Am. Chem. Soc. 124 (2002) 6119.
[39] K. Möller, J. Kobler, T. Bein, J. Mater. Chem. 17 (2007) 624.
[40] B. Xu, Y. Hao, H. Wang, H. Zhou, X. Liu, M. Chen, Solid State Commun. 136 (2005) 318.
[41] D.H. Everett, Pure Appl. Chem. 31 (1972) 577.
[42] H. Okabayashi, K. Izawa, T. Yamamoto, H. Masuda, E. Nishio, C.J. O'Connor, Colloid Polym. Sci. 280 (2002) 135.
[43] T. Gavrilko, R. Fedorovich, G. Dovbeshko, A. Marchenko, A. Naumovets, V. Nechytaylo, G. Puchkovska, L. Viduta, J. Baran, H. Ratajczak, J. Mol. Struct. 704 (2004) 163.
[44] K. Wilson, A.F. Lee, D.J. Macquarrie, J.H. Clark, Appl. Catal. A 228 (2002) 127.
[45] C. Despas, A. Walcarius, J. Bessiére, Langmuir 15 (1999) 3186.
[46] J. Gao, C. Lü, X. Lü, Y. Du, J. Mater. Chem. 17 (2007) 4591.